Published in final edited form as:
Eur J Neurosci. 2012 February ; 35(3-4): 562–571. doi:10.1111/j.1460-9568.2011.07972.x.

Genetic inactivation of p66ShcA is neuroprotective in a murine model of multiple sclerosis

Kimmy G. Su[1], **Costanza Savino**[3], **Gail Marracci**[1,2], **Priya Chaudhary**[1], **Xiaolin Yu**[1], **Brooke Morris**[1], **Danielle Galipeau**[1], **Marco Giorgio**[3], **Michael Forte**[*,1], and **Dennis Bourdette**[*,1,2]

[1]Oregon Health & Science University, 3181 SW Sam Jackson Park Rd, Portland, OR 97239

[2]Portland VA Medical Center, 3710 SW US Veterans Hospital Rd, Portland, OR, 97239

[3]European Institute of Oncology, Milan, Italy 20141

Abstract

Although multiple sclerosis (MS) has traditionally been considered an inflammatory disease, recent evidence has brought neurodegeneration into the spotlight, suggesting that accumulated damage and loss of axons is critical to disease progression and associated irreversible disability. Proposed mechanisms of axonal degeneration in MS posit cytosolic and subsequent mitochondrial Ca^{2+} overload, accumulation of pathologic reactive oxygen species (ROS), and mitochondrial dysfunction leading to cell death. In this context, the role of protein p66ShcA (p66) may be significant. The ShcA isoform is uniquely targeted to the mitochondrial intermembrane space in response to elevated oxidative stress, and serves as a redox enzyme amplifying ROS generation in a positive feed-forward loop that eventually mediates cell death by activation of the mitochondrial permeability transition pore (PTP). Consequently, we tested the hypothesis that genetic inactivation of p66 would reduce axonal injury in a murine model of MS, experimental autoimmune encephalomyelitis (EAE). As predicted, the p66-KO mice developed typical signs of EAE, but had less severe clinical impairment and paralysis compared to WT mice. Histologic examination of spinal cords and optic nerves showed significant axonal protection in the p66-KO tissue despite similar levels of inflammation. Furthermore, cultured p66-KO neurons treated with agents implicated in MS neurodegenerative pathways showed greater viability compared to WT neurons. These results confirm the critical role of ROS-mediated mitochondrial dysfunction in the axonal loss that accompanies EAE and identify p66 as a new pharmacologic target for MS neuroprotective therapeutics.

Keywords

p66ShcA; EAE; multiple sclerosis; neurodegeneration; neuroprotective; mitochondria

II. Introduction

Multiple sclerosis (MS) is the most common chronic inflammatory disease of the central nervous system (CNS) affecting more than 2 million people worldwide (Noseworthy et al., 2000). Pathologic immune responses have long been viewed as the primary mediator of MS, leading to the development of anti-inflammatory drugs moderately successful in treating

[*]Co corresponding authors Address correspondence to: Michael Forte Vollum Institute, L474 Oregon Health and Science University 3181 SW Sam Jackson Park Road Portland, OR 97239 Phone: (503) 494-5454 FAX: (503) 494-4976 forte@ohsu.edu.

Author contributions: K.G.S, M.F., D.B., M.G. designed research; K.G.S., C.S., G.M., P.C., X.Y., B.M., D.G. performed research; K.G.S. analyzed data; K.G.S., M.F., D.B. wrote the paper.

relapsing-remitting forms of the disease (Lublin, 2005). Unfortunately, these drugs have minimal impact on neurodegeneration that is now believed to contribute to the permanent disability associated with progressive forms of MS. Effective treatment for progressive MS will likely require neuroprotective therapies targeting the underlying mechanisms of axonal degeneration.

Growing evidence suggests that MS neurodegeneration revolves around mitochondrial dysfunction (Dutta et al., 2006; Mahad et al., 2008). Various pathways leading to such dysfunction have been proposed, and upstream drives of mitochondrial dysfunction have been identified in both MS and the murine disease model experimental autoimmune encephalomyelitis (EAE) (Craner et al., 2004a; Craner et al., 2004b). Interestingly, these various pathways all at some level postulate pathologic opening of the permeability transition pore (PTP) located in the inner mitochondrial membrane (Su et al., 2009). Specifically, mitochondrial Ca^{2+} overload and pathologic ROS generation opens the PTP, and persistent opening can initiate detrimental disruption of mitochondrial structure and function and induce cell death (Bernardi et al., 2006). Accordingly, we, and others, have suggested that PTP activation potentially mediates neurodegeneration in MS and other neurologic diseases (Rasola and Bernardi, 2007; Forte et al., 2007).

While the structure of the PTP is poorly understood, there is solid evidence that the mitochondrial matrix protein cyclophilin D (CyPD) plays a crucial regulatory role for the pore (Baines et al., 2005; Basso et al., 2005). CyPD inhibition by pharmacologic and genetic techniques is protective in disease models of ischemic and traumatic brain injury as well as various human neurodegenerative conditions (Schinzel et al., 2005). In particular, CyPD inhibition was shown to be neuroprotective in the murine MS model EAE (Forte et al., 2007). CyPD-knockout (CyPD-KO) mice showed significant clinical improvement following the development of paralysis unlike the wild type (WT) mice. Furthermore, there was decreased axonal damage and loss in the CyPD-KO spinal cords despite similar levels of inflammatory cells compared to the WT mice. These results support the hypothesis that modulation of PTP opening may protect axons from injury in EAE.

Additional physiologic triggers of PTP opening include ROS exposure, and accordingly, the ShcA isoform p66 has been proposed as a potential upstream pore modulator (Migliaccio et al., 1999). In the presence of pathologic ROS levels, p66 is uniquely targeted to the mitochondrial intermembrane space by protein kinase Cβ (PKCβ)-mediated serine phosphorylation (Pinton et al., 2007). There, it serves as a redox enzyme by oxidizing cytochrome c and reducing oxygen to form ROS including superoxide and hydrogen peroxide (Giorgio et al., 2005). This source of mitochondrial ROS constitutes a positive feed-forward loop that is thought to induce pathologic PTP opening leading to mitochondrial dysfunction and eventual cell death. Several groups have shown that p66 inhibition confers protection to oxidative stress in various experimental contexts and disease models (Migliaccio et al., 1999; Camici et al., 2007). Based on this information, we tested the hypothesis that p66-KO mice would demonstrate axonal preservation following EAE induction.

III. Materials and methods

Animals

p66-KO, CyPD-KO, and p66/CyPD double knockout (p66/CyPD-DKO) mice were maintained as homozygotes in a C57BL/6 background (Migliaccio et al., 1999). Isogenic WT C57BL/6 mice were obtained from The Jackson Laboratory (Bar Harbor, ME) and Taconic Farms (Germantown, NY). All experimental procedures were conducted following

NIH guidelines under an Institutional Animal Care and Use Committee-approved protocol from the Oregon Health & Science University.

Western blots of nervous tissue and neurons

Expression of p66 was examined in lysates prepared from brain cortices and hippocampal neurons. Lysates were immunoprecipitated with anti-Shc antibody (BD Biosciences, San Jose, CA) on precleared protein G beads, and examined by immunoblot analysis using the BG8 monoclonal anti-p66Shc antibody (Orsini et al., 2004). Membranes were stripped and re-probed to detect beta-tubulin as a protein loading control.

EAE immunization and clinical scoring

Isogenic 10–12 week-old female mice were immunized by subcutaneous injection with myelin oligodendrocyte glycoprotein (MOG) 35-55 peptide (200 μg) in complete Freund's adjuvant containing *M. tuberculosis* (400 μg) per mouse. Pertussis toxin was administered intraperitoneally following immunization (75 ng/mouse) and again 48 hours later (200 ng/mouse). Mice were scored daily for EAE by using a 9-point scale [0, no paralysis; 1, limp tail with minimal hind limb weakness (easily flipped onto their backs with a twist of the tail but able to easily right themselves); 2, mild hind limb weakness (difficulty righting themselves after being flipped on their back); 3, moderate hind limb weakness (able to walk with no difficulty but unable to right themselves after being flipped on their backs); 4, moderately severe hind limb weakness (difficulty walking upright); 5, severe hind limb weakness (unable to walk upright but still able to move hindlimbs); 6, complete hind limb paralysis (no voluntary leg movement); 7, hind limb paralysis with mild forelimb weakness (walks with chest close to the ground); 8, hind limb paralysis with moderate forelimb weakness (unable to lift chest off the ground but can move around cages with difficulty); and 9, hind paralysis with severe forelimb weakness (unable to place forelimbs under chest and unable to move around cage)] (Marracci et al., 2002; Forte et al., 2007). Scoring was performed blinded to genotype. After 36 days of clinical assessment, the mice were deeply anesthetized with isoflurane, heparinized, and perfused with ice-cold 4% paraformaldehyde. Spinal cords and optic nerves were dissected out the following day for processing, sectioning, and analysis (see details below). For the representative p66-KO and WT experiment reported in the results, 8 p66-KO mice and 18 WT mice were immunized and analyzed for clinical EAE. All mice with EAE were perfused for further histologic analyses along with 3 naïve mice per genotype. For the single and double mutant comparative experiment, 7 p66-KO, 15 CyPD-KO, and 8 p66/CyPD-DKO mice were immunized and assessed along with 3 naïve mice per genotype. For the early time-point (day 16 post-immunization) assessment of immune cell infiltration, 7 p66-KO mice and 8 WT mice were immunized and assessed along with 2 naïve mice per genotype.

Quantitative morphologic analysis of percent white matter tissue damage

Thoracic spinal cord white matter—Thoracic spinal cord blocks were immersed in 5% glutaraldehyde for 3 days and post-fixed with 1% osmium tetroxide. Semithin sections (0.5 μm) were stained with toluidine blue and photographed at 20× magnification to create photomontages of the spinal cord cross-sections. One cross-section photomontage was generated per mouse. Quantification of the percentage of white matter tissue damage in the ventrolateral region was determined by manually marking the photomontages (digitally magnified on monitor to 40×) utilizing Image J software. Total ventrolateral area was determined by circling the entire ventrolateral region of the thoracic spinal cord cross section. Marked damage included areas devoid of axons or areas containing swollen axons, degenerating axons, demyelinated axons, irregularly myelinated axons, myelin ovoids, or microcysts. The percentage of area damaged in the ventrolateral region for each thoracic

section was determined using the following formula: (total marked damaged area)/(total ventrolateral area) × 100. All analyses were done blinded to genotype.

Optic nerve—Optic nerves were immersed in 5% glutaraldehyde overnight and post-fixed with 1% osmium tetroxide. Semithin sections (0.5 μm) were stained with toluidine blue and photographed at 100× magnification to create photomontages of the optic nerve cross-sections. One cross-section photomontage was generated for each mouse. The percentage of area damaged was quantified by manually marking the photomontages at 100× utilizing Image J software. The total cross-sectional area was determined by outlining the entire optic nerve, and damage was manually marked based on the same criteria described for the spinal cord white matter. The percentage of area damaged for each optic nerve section was determined by the following formula: (total marked damaged area)/(total cross-sectional area) × 100. All analyses were done blinded to genotype.

Axonal count of thoracic spinal cord ventrolateral white matter

For each plastic-embedded, toluidine blue-stained spinal cord section, a total of 8 images (4 on either side of the cord midline) were taken of the ventrolateral white matter at 20× magnification. The area of each image was 344 × 258 μM^2. Utilizing Metamorph software (Molecular Devices, CA), each image was first thresholded to maximize the number of axon cross-sections highlighted. Next, the integrated morphometry analysis measurement parameters of area, shape factor, and elliptical form factor were applied to the thresholded regions to generate an initial axon count for the image. False positive axons and highlighted damaged axons were manually subtracted from this initial axon count to determine the final axon count for the image. All analyses were done blinded to genotype.

Electron microscopy

Ultrathin plastic embedded thoracic spinal cord and optic nerve sections (70 nm) were collected on copper grids and stained with uranyl acetate and lead citrate. Stained sections were examined at 4800× and 9300× using a JEOL or an FEI Tecnai 12 electron microscope, and images were captured using a digital camera (Advanced Microscopy Techniques (AMT) Corporation, Danvers, MA, USA). All analyses were done blinded to genotype.

Analysis of immune cell infiltration

Lumbar spinal cord—Spinal cord blocks were embedded in 3% agarose and sectioned (50μm) using a Leica Vibratome (Leica Microsystems, Nussloch, Germany). Three sections from each lumbar spinal cord region were randomly selected for antibody staining. Sections were permeabilized, washed, and blocked (0.5% fish skin gelatin/3% BSA in PBS), and then incubated with primary antibody at 4°C overnight. Primary anti-CD4 antibody (PharMingen, San Diego, CA) was used to identify T cells, and anti-CD11b (Leinco Technologies, St. Louis, MO) was used as a microglial/macrophage marker. The following day, the sections were washed and incubated in secondary Alexa Fluor 488 conjugated donkey anti-rat IgG (Invitrogen, Carlsbad, CA) at room temperature for 1.5 hours. Following a final wash, the sections were mounted on slides in Prolong Gold Antifade, and imaged using a laser scanning Zeiss LSM710 confocal microscope (LSM-710, Carl Zeiss, Göttingen, Germany). Four images of each lumbar section (dorsal, ventral, and two lateral regions) were photographed at 40×. Two sections were photographed per mouse. Data analyses were performed using Metamorph software (Molecular Devices, CA). The amount of fluorescence per image was determined by generating the percent threshold area, and the average background fluorescence was accounted for by analyzing the negative controls, which included sections from naïve and EAE-induced mice incubated with primary antibody

only, secondary antibody only, or neither antibody. All analyses were done blinded to genotype.

Optic nerves—Optic nerves were sectioned, stained and mounted in the same manner as the lumbar spinal cords. Entire stained sections were imaged at 40× by confocal microscopy. Quantification of CD4 and CD11b fluorescence per section was carried out by determining the threshold percentage for a standard area of about 20,000 μM^2. All analyses were done blinded to genotype.

Proliferation and cytokine studies

WT and p66-KO 10–12 week old female mice were immunized with MOG 35-55 peptide as described above to induce EAE. At ten days post-immunization, the mice were euthanized by CO_2 inhalation and inguinal lymph nodes (LN) were harvested to establish cell cultures following previously described methods (Marracci et al. 2002). LN cultures were incubated with IL-2, MOG 35-55 peptide (25μg/mL) or media. The data reported reflects two independent experiments (n of 5 mice/genotype per experiment).

Cytokine assay—After 48 hours of incubation at 37°C, LN culture supernatants were collected and frozen at −80°C until used for cytokine assays. The Luminex Bio-Plex mouse cytokine assay kit (Bio-Rad, Hercules, CA) was used to analyze the following cytokines per manufacturer's protocol: IL-2, IL-4, IL-6, IL-10, IL-17, IFN-gamma, and TNF-alpha.

Proliferation assay—After 48 hours of incubation at 37°C, LN cells were labeled with [^{3}H] thymidine and returned to the incubator for 18 hours. The cells were then harvested onto glass fiber filtermats and assessed for uptake of the labeled thymidine by liquid scintillation per manufacturer's protocol (Perkin Elmer-Wallac, Waltham, MA).

In vitro neuronal culture studies

Cortical neurons were obtained from dissected brains of WT and p66-KO animals as previously outlined (Barsukova et al., 2011). Immunocytochemical analysis indicated that the majority of cells in these adult preparations (>70%) were neurons with characteristic morphology. The cells were counted, resuspended in culture medium [B27/Neurobasal A medium/0.5 mM glutamine (Invitrogen, Carlsbad, CA) supplemented with 50 mg/L gentamicin (Sigma, St. Louis, MO)] and seeded at high density into 24 well plates pre-coated overnight with 10 μg/mL poly-d-lysine (Sigma, St. Louis, MO). The neuronal cultures were maintained for one week before experimental manipulation. Prior to treatment with either diethylenetriamine/nitric oxide adduct (DETA-NO) or H_2O_2 (Sigma, St. Louis, MO), the cells were washed with Neurobasal A medium/0.5 mM glutamine. Half of the 24 wells were designated control wells and treated with Neurobasal A medium/0.5 mM glutamine. The other half were designated treatment wells and treated with either 500 μM DETA-NO or 200 μM H_2O_2. Following a treatment period of 15 minutes in a 37 °C incubator, the cells were washed twice in Neurobasal A medium/0.5 mM glutamine and returned to the incubator in fresh culture medium. Neuronal viability was assessed 24 hours later by incubating the cells in Calcein AM (AnaSpec, San Jose, CA) and manually counting live neurons based on morphologic appearance and presence of green fluorescent dye at 20× with a fluorescence inverted microscope. Four random areas were counted per well, for a total of 48 random areas counted per treatment or control group per plate. The cell viability percentage was calculated per plate as follows: live cell count in treatment group/live cell count in control group × 100. All analyses were done blinded to genotype.

Statistics

All statistical comparisons between the p66-KO and WT groups were calculated using the nonparametric Mann-Whitney U test. Statistical comparison among p66-KO, CyPD-KO, and p66/CyPD-DKO mice was calculated using the one-way ANOVA for 3 independent samples. Statistical significance was defined as $p<0.05$.

IV. Results

p66 expression in WT and p66-KO nervous tissue and neurons

Three protein isoforms, p46, p52, and p66, are generated from the mammalian *ShcA* locus and share common phosphotyrosine-binding (PTB), Src homology 2 (SH2) and collagen homology (CH1) domains (Migliaccio et al., 1999). The p46 and p52 isoforms participate in the transduction of signals from activated tyrosine kinases at the plasma membrane. In comparison, the p66 isoform contains a N-terminal extension that includes unique CH2 and cytochrome c-binding domains as well as an atypical mitochondrial targeting sequence. Consequently, up to 40% of p66 is localized to mitochondria (Orsini et al., 2004; Nemoto et al., 2006). Cellular ROS exposure results in the stimulation of p66 expression and the stabilization of existing p66. Newly formed p66 is phosphorylated by PKCβ in the cytosol, which allows for conformational modification by the prolyl isomerase PIN1 (Pinton et al., 2007). Modified p66 is then translocated into the mitochondrial intermembrane space to supplement existing levels of mitochondrial p66. Following dephosphorylation within the intermembrane space, p66 functions as a redox enzyme interacting with cytochrome c to amplify ROS levels that generate a positive feed-forward loop (Giorgio et al., 2005; Gertz and Steegborn, 2010a).

Since the mammalian *ShcA* gene encodes two mRNA species via alternate translation start sites specific for p66 and p46/p52, it has been possible to generate mice exclusively missing p66 while retaining expression of the two other isoforms. While p66 expression has already been demonstrated in neuronal cell lines from different mammalian species (Smith et al., 2005; Giorgio et al., unpublished), we initially confirmed p66 expression and elimination in the nervous tissue and neurons of the animals used in the present study. Immunoblot analyses of lysates prepared from p66-KO and WT mouse brain cortices and hippocampal neurons (Figure 1) demonstrated p66 expression in lysates prepared from WT animals and the absence of p66 in lysates prepared from p66-KO animals.

p66 elimination protects axons in EAE

Our previous work on CyPD-KO mice showed significant axonal protection following EAE induction (Forte et al., 2007), suggesting that regulation of the PTP and mitochondria-directed cell death may be key to preventing degenerative pathways. If p66 lies upstream of PTP activation and thereby mediates cell death via mitochondrial ROS generation, one would expect the elimination of p66 to confer similar protection in mice with EAE. To test this hypothesis, we assessed clinical severity and extent of axonal damage following EAE induction in p66-KO mice compared to WT mice. Subsequent to immunization with MOG 35-55 peptide, both WT and p66-KO mice developed clinical signs of EAE. However, the p66-KO mice exhibited less severe clinical disease compared to the WT mice. Throughout the entire 36-day observation period, the p66-KO mice had consistently lower mean EAE scores compared to the WT mice. Furthermore, at the end of this period, the p66-KO mice had significantly lower mean EAE scores (p66-KO 2.2±0.6, WT 3.6±0.5; $z= 1.80556$; $p=0.035$), reflecting the consistent trend of reduced clinical impairment (Figure 2).

Following the 36-day observation period, spinal cords and optic nerves were collected for histologic analyses, including the quantification of tissue damage. EAE-induced tissue

damage in C57BL/6 mice typically manifests as degenerating axons and reduced axonal density and is particularly prominent in the ventrolateral spinal cord white matter. Accordingly, we assessed tissue integrity in plastic-embedded thoracic spinal cord sections stained with toluidine blue. Analysis of ventrolateral thoracic spinal cord white matter showed significantly less damage in the p66-KO mice compared to the WT mice. The WT mice had a mean damaged area of 21.9±2.3%, exhibiting prominent pathological changes including swollen axons, degenerating axons, demyelinated axons, irregularly myelinated axons, myelin ovoids, microcysts, and areas devoid of axons. By comparison, the p66-KO mice showed significantly less damage with a mean damaged area of 12.7±2.6%, indicating a 42% reduction in ventrolateral white matter damage ($z= 2.38889; p=0.008$) (Figure 3A–C).

To further analyze the effects of p66 elimination on axonal integrity, an axonal count was performed in a sampling of images taken of toluidine blue-stained thoracic spinal cord sections. Unlike the results reported above, which assessed total tissue damage within the entire ventrolateral region including degenerating axons, demyelinated axons, and areas devoid of axons, this analysis focused on counting the number of intact axons within a sample area of the white matter region. The results indicated that within each sampled image (344 μm × 258 μm), the average axon count was 4719.89±158 for the p66-KO mice compared to 4352.84±99 for the WT mice. This difference was found to be statistically significant ($z=1.74471; p=0.041$), suggesting that p66 elimination preserves white matter in mice with EAE by limiting the extent of generalized tissue damage as well as preserving the number of intact axons.

Given the proposed connection between mitochondrial p66-generated ROS and PTP activation, we also assessed the stability of spinal cord axons by the approaches outlined above in p66/CyPD double mutant mice lacking both p66 and CyPD. We found no significant differences in their clinical presentation of EAE ($F_{2,30}=0.4873; p=0.62$) and in the amount of ventrolateral damage in the double mutants as compared to either single mutant. The p66-KO mice had a mean of 13.2±2.9% damage in the spinal cord, compared to 15.7±1.2% for the CyPD-KO mice, and 11.8±1.5% for the p66/CyPD-DKO mice ($F_{2,27}=1.52; p=0.237$).

In addition, most C57BL/6 mice with EAE also have inflammation and axonal degeneration in their optic nerves similar to optic neuritis seen in patients with MS (Chaudhary et al., 2011). Optic nerves stained with toluidine blue were assessed for axonal injury and were found to be protected in the p66-KO mice in a similar manner to that shown in the spinal cords. There was a significant 38% reduction in damage observed in the optic nerves of p66-KO mice as compared to WT mice (p66-KO 23.4±3.1%, WT 37.5±3.6%; $z=2.79625; p=0.0026$) (Figure 3D–F).

Finally, to capture a magnified depiction of the axonal protection observed in the thoracic spinal cords and optic nerves, electron microscopy was performed on ultra-thin plastic toluidine blue-stained tissue sections. As shown in Figure 4, there was a striking contrast in axonal morphology between the p66-KO and WT sections. In particular, the WT sections had multiple axons with noticeably abnormal structural characteristics including myelin ovoids without discernible axons and large swollen axons containing membranous debris. Similar structural abnormalities were found in the electron microscopic analysis of optic nerve sections.

Overall, the results from our multidimensional analysis of axonal integrity in p66-KO and WT mice with EAE indicate significant neuroprotection associated with p66 elimination. Tissue and axonal preservation was apparent in CNS regions relevant to MS pathology,

including the optic nerves that are commonly symptomatic and damaged in MS patients. These findings are consistent with the hypothesis that p66 operates upstream of PTP activation in MS degenerative disease processes.

EAE immune cell infiltration is similar in WT and p66-KO mice

The development of EAE in the C57BL/6 mouse background is dependent on the activation of CD4+ T cells and CD11b+ macrophages/microglia in the CNS following MOG 35-55 peptide immunization. Therefore, it is possible that the reduction in axonal damage observed in the p66-KO mice might have reflected a dampened immune response to the MOG-induced EAE. To investigate this possibility, the infiltration of immune cells within spinal cord and optic nerve tissue was assessed at both early (day 16 post-immunization) and late (day 36 post-immunization) time-points.

Lumbar spinal cord sections were immunostained for inflammatory cells using anti-CD4 and anti-CD11b to identify T cells and microglia/macrophages, respectively. As expected, elevated CD4 and CD11b immunofluorescence levels were observed in both p66-KO and WT mice compared to naïve non-immunized controls of both genotypes. Analysis of fluorescence levels by percent threshold area showed no statistically significant differences in CD4 and CD11b staining between p66-KO and WT mice at both early and late time-points. At day 16 post-immunization, the p66-KO and WT mice had similar mean EAE scores (p66-KO 5.43±0.30, WT 5.77±0.25; $z=0.58284$; $p=0.28$), and correspondingly, no significant differences in CD4 (p66-KO 2.21±0.22%, WT 2.62±0.23%; $z=0.77219$; $p=0.22$) and CD11b (p66-KO 9.69±1.25%, WT 12.52±1.45%; $z=0.52440$; $p=0.30$) staining. At day 36 post-immunization, immune cell infiltration was also found to be similar between the p66-KO and WT mice with EAE for both CD4 (p66-KO 1.00±0.09%, WT 1.04±0.09%; $z=1.44656$; $p=0.07$) and CD11b (p66-KO 9.35±0.80%, WT 8.66±0.49%; $z=0.41116$; $p=0.34$) staining (Figure 5A–D).

Immune cell infiltration was also assessed in optic nerves by CD4 and CD11b staining. Similar to the results in the lumbar spinal cords, the optic nerves of p66-KO and WT mice had elevated CD4+ T cell and CD11b+ macrophage/microglia infiltration compared to the naïve non-immunized controls of both genotypes at both early and late time-points. Importantly, as in lumbar spinal cords, no significant differences were observed at day 16 post-immunization for neither CD4 (p66-KO 2.63±0.53%, WT 2.24±0.25%; $z=0.52440$; $p=0.70$) nor CD11b (p66-KO 8.36±1.89%, WT 6.43±0.78%; $z=0.80642$; $p=0.79$) staining in p66-KO and WT mice with EAE. Similarly, neither CD4 (p66-KO 1.04±0.14%, WT 0.92±0.10%; $z=0.81016$; $p=0.21$) nor CD11b (p66-KO 21.76±1.35%, WT 20.69±1.27%; $z=0.63424$; $p=0.26$) staining was statistically different at day 36 post-immunization (Figure 5E–H).

Overall, a comparable inflammatory response in the two genotypes was shown in the spinal cord and optic nerve sections at both early and late time-points following EAE onset. This suggests that the axonal protection observed in the p66-KO mice was not primarily due to a reduced immune response to the MOG peptide immunization subsequent to the elimination of p66.

p66-KO and WT T-cells proliferate similarly in response to MOG 35-55 peptide

Although the immunohistochemical quantification of immune cell infiltration was found to be similar at both early and late time-points following EAE onset, it is possible that immune responses to MOG 35-55 peptide might be attenuated in the p66-KO mice. Therefore, to further compare the immune response in p66-KO and WT mice during the early phases of EAE, T-cell proliferation and cytokine studies were performed. T-cell proliferation studies

were carried out on mice immunized with MOG 35-55 peptide 10 days following induction of EAE using the standard protocol. The results indicated no significant difference in proliferative responses between the p66-KO and WT groups, which exhibited similar stimulation indexes (stimulated/unstimulated) for the positive control IL-2 (p66-KO 18.14±0.02, WT 18.04±3.97; *z=0.96077; p=0.17*) and MOG 35-55 peptide (p66-KO 4.65±1.61, WT 4.35±3.28; *z=0; p=0.50*) (Figure 6). The comparable T-cell proliferation between the p66-KO and WT lymph node cultures confirms a similar response to the EAE immunization as shown by immunohistochemical staining for CD4+ T-cells (Figure 5). Moreover, these results suggest that immunoreactivity and infiltration capacity is unaltered between the early (day 10) and late stages (day 36) of EAE. These results further indicate that the neuroprotection shown in the p66-KO mice is not attributable to significant differences in T-cell responses to MOG 35-55 peptide.

Activated p66-KO and WT T-cells produce similar cytokine levels

A final comparative analysis of cytokine levels produced by p66-KO and WT lymph node cultures stimulated with MOG 35-55 peptide indicated no significant differences, further supporting the aforementioned results of similar immunoreactivity during the EAE induction period. Specifically, measured levels of proinflammatory Th1 (TNF-alpha, IFN-gamma), Th2 (IL-4, IL-10), and Th17 (IL-17) cytokine levels were not found to be significantly different between the two genotypes (Table 1a–c). Overall, the cytokine levels detected following MOG 35-55 activation of lymph node cultures from immunized mice provided further confirmation that T-cell immunoreactivity was similar between the p66-KO and WT mice at an early stage of EAE.

Isolated p66-KO neurons are protected in the presence of agents implicated in MS neurodegenerative pathways

Pathologic levels of reactive oxygen and nitrogen species are proposed to mediate mitochondrial dysfunction and ensuing axonal damage in EAE and MS neurodegenerative pathways (Su et al., 2009). Accordingly, we examined the potential protective effects of p66 elimination in neurons by utilizing a controlled *in vitro* neuronal culture system and treatment application of either 500μ-M DETA-NO or 200 μ-M H_2O_2. Our results showed that p66-KO cortical neuronal cultures had significantly greater resistance to both treatments compared to the WT neuronal cultures (Figure 7). The results are consistent with the hypothesis that the axonal protection observed in p66-KO mice with EAE is due to enhanced protection from inflammatory mediators of axonal damage via modulated mitochondrial ROS production.

V. Discussion

In this report, we demonstrated that induction of EAE in p66-KO mice resulted in less severe clinical disease compared to WT mice and reduced axonal damage without a reduction in inflammation within the spinal cord and optic nerves. While the clinical protection may not be as robust as our previous studies in CyPD-KO mice (Forte et al., 2007), it is important to note that clinical EAE is largely reflective of inflammation in the spinal cord in response to MOG peptide immunization rather than the extent of axonal damage (Wujek JR et al., 2002). Similarly, in MS, early clinical signs include increased weakness, paralysis, visual impairment, and other disabilities, which are more often due to an active inflammatory attack on the nervous system (Steinman L, 2001).

Therefore, histologic analysis of spinal cord and optic nerve tissue from mice with EAE is a better gauge of the potential neuroprotective effects incurred by p66-KO mice. Our results demonstrated a significant reduction in axonal degeneration from both spinal cord and optic

nerve tissue. Notably, the extent of infiltration by CD4+ and CD11b+ cells of spinal cords and optic nerves was not significantly different between p66-KO and WT mice with EAE. Although it is possible that the immune response in the p66-KO mice might be qualitatively different, the peripheral immune responses to MOG 35-55 peptide, including pro-inflammatory and regulatory cytokine production, did not differ between the p66-KO and WT mice, supporting the notion that the protective effects in the p66-KO mice with EAE were not secondary to an altered immune response. Increased viability *in vitro* of p66-KO neuronal cultures following incubation with EAE- and MS-associated neurodegenerative agents (i.e., NO, H_2O_2) further confirmed the protective effects acquired by loss of p66. Given that p66 is a mediator of PTP opening and cell death via mitochondrial ROS generation, these findings provide further support for our hypothesis that PTP activation is critical to axonal degeneration in EAE, and by implication, MS (Forte et al., 2007). Our results establish the importance of p66 in mediating axonal injury in EAE and are the first to examine the role of p66 and the significance of its absence in a murine model of a human neurologic disorder.

The experiments reported here focus on the p66 ShcA isoform as part of a signaling network that contributes to stress responses, lifespan regulation, and aging through its role of ROS generation within the mitochondrial intermembrane space. Various studies, primarily those using isolated mitochondrial preparations, have supported a model in which a “ROS stress-sensing complex” keeps p66 inactive as long as stress levels remain moderate (Gertz and Steegborn, 2010b). However, under conditions of increased cellular stress as accompanies ischemia and many neurological diseases, including MS, p66 has been proposed to function in a positive feed-forward loop by oxidizing cytochrome c and reducing oxygen to form ROS, which then trigger the initiation of mitochondrial dysfunction and PTP-dependent cell death. Consequently, our results are consistent with the concept that the PTP may constitute the immediate downstream target of mitochondrial p66 action in cell death pathways, and similarly are consistent with the recent demonstration that superoxide may be one of the key triggers for PTP opening *in situ* (Wang et al., 2008). Furthermore, p66-KO mice have been shown to be resistant to cell death resulting from a number of stresses (ex: UV, ROS) and notably exhibit a 30% increase in lifespan (Migliaccio et al., 1999).

The impact of p66 action on mitochondria-mediated cell death and neurodegenerative mechanisms likely goes beyond MS and extends to other neurodegenerative conditions such as stroke, Alzheimer's disease (AD), and amyotrophic lateral sclerosis (ALS). Evidence suggests that these diseases progress in part due to deleterious effects on mitochondrial function, including disruption of the electron transport chain, excessive ROS production, altered mitochondrial homeostasis, and pathologic PTP opening (Lin and Beal, 2006; Su et al., 2009). In particular, CyPD-KO mice demonstrate that repression of PTP activation confers protection in ALS (Martin et al., 2009), AD (Du et al., 2008), and stroke (Schinzel et al., 2005) as well as MS. Furthermore, amyloid β-peptide modulation of p66 serine phosphorylation and apoptosis in SH-SY5Y human neuroblastoma and other neuronal cell lines suggests that p66 may play a significant role in AD neurodegeneration (Smith et al., 2005).

Our work emphasizes the importance of identifying pharmacologic targets that can modulate the mitochondrial PTP, such as CyPD, and in this study, p66, for the development of neuroprotective treatments for MS and potentially other neurodegenerative diseases. Currently, mitochondria-directed therapies are still in their infancy, largely limited to *in vitro* and *in vivo* animal studies to test their properties and efficacy, although a few are now being investigated in human clinical trials. They span a wide range of mitochondria-specific targets including the electron transport chain, ATP synthase, mitochondrial ROS, and the PTP (Camara et al., 2009; Moreira et al., 2010). The effectiveness of these mitochondria-

targeted drugs in treating MS will depend on multiple factors, including the ability of the drug to accumulate within the CNS and to achieve therapeutic levels within mitochondria. Unlike many other organ systems, CNS drug delivery can be difficult due to the restrictive blood brain barrier. Cyclosporin A and its non-immunosuppressive derivatives, for instance, are highly effective in blocking the PTP, but are limited in their effectiveness as neuroprotectants due to poor CNS penetration (Begley et al., 1990). Therefore, drug modification and utilization of barrier-permeable delivery vehicles may need to be taken into consideration. In addition, drug accumulation within the mitochondria will be crucial to drug design and potential effectiveness.

In summary, we have provided novel evidence pinpointing p66 as a neuroprotective target in the MS disease model EAE. As we gain a better understanding of this redox enzyme and its role as a mitochondria-targeted signaling molecule mediating cell death, it may prove to be an ideal drug target in the development of neuroprotective treatments not only for MS, but for other neurodegenerative diseases as well.

Acknowledgments

We thank the members of the Forte and Bourdette labs for their excellent technical assistance. This work was supported by grants from the National Institutes of Health (P30-NS0693464, GM-069883, NS-057433, F30-NS704792), the National MS Society, the Tartar Trust, the OHSU Brain Institute, the Laura Fund for Innovation in Multiple Sclerosis, and the Department of Veterans Affairs, Veterans Health Administration, Office of Research and Development, Biomedical Laboratory Research and Development. The contents do not represent the views of the Department of Veterans Affairs or the US government.

VII. Abbreviations

CNS	central nervous system
CsA	cyclosporin A
CyPD	cyclophilin D
CyPD-KO	cyclophilin D-knock out ($Ppif^{-/-}$)
DETA-NO	diethylenetriamine/nitric oxide adduct
EAE	experimental autoimmune encephalomyelitis
LN	lymph node
MOG	myelin oligodendrocyte glycoprotein
MS	multiple sclerosis
NO	nitric oxide
p66	p66ShcA
p66-KO	p66-knock out
p66/CyPD-DKO	p66/CyPD-double knock out
PKCβ	protein kinase Cβ
PTP	permeability transition pore
ROS	reactive oxygen species
WT	wild-type

VIII. References

Baines CP, Kaiser RA, Purcell NH, Blair NS, Osinska H, Hambleton MA, Brunskill EW, Sayen MR, Gottlieb RA, Dorn GW, Robbins J, Molkentin JD. Loss of cyclophilin D reveals a critical role for mitochondrial permeability transition in cell death. Nature. 2005; 434:658–662. [PubMed: 15800627]

Barsukova A, Komarov A, Hajnóczky G, Bernardi P, Bourdette D, Forte M. Activation of the mitochondrial permeability transition pore modulates Ca2+ responses to physiological stimuli in adult neurons. European Journal of Neuroscience. 2011; 33:831–842. [PubMed: 21255127]

Basso E, Fante L, Fowlkes J, Petronilli V, Forte MA, Bernardi P. Properties of the Permeability Transition Pore in Mitochondria Devoid of Cyclophilin D. Journal of Biological Chemistry. 2005; 280:18558–18561. [PubMed: 15792954]

Begley DJ, Squires LK, Zloković BV, Mitrović DM, Hughes CCW, Revest PA, Greenwood J. Permeability of the Blood-Brain Barrier to the Immunosuppressive Cyclic Peptide Cyclosporin A. Journal of Neurochemistry. 1990; 55:1222–1230. [PubMed: 2398356]

Bernardi P, Krauskopf A, Basso E, Petronilli V, Blalchy-Dyson E, Di Lisa F, Forte MA. The mitochondrial permeability transition from in vitro artifact to disease target. FEBS Journal. 2006; 273:2077–2099. [PubMed: 16649987]

Camara AKS, Lesnefsky EJ, Stowe DF. Potential Therapeutic Benefits of Strategies Directed to Mitochondria. Antioxidants & Redox Signaling. 2009; 13:279–347. [PubMed: 20001744]

Camici GG, Schiavoni M, Francia P, Bachschmid M, Martin-Padura I, Hersberger M, Tanner FC, Pelicci P, Volpe M, Anversa P, Lüscher TF, Cosentino F. Genetic deletion of p66Shc adaptor protein prevents hyperglycemia-induced endothelial dysfunction and oxidative stress. Proceedings of the National Academy of Sciences. 2007; 104:5217–5222.

Carpi A, Menabò R, Kaludercic N, Pelicci P, Di Lisa F, Giorgio M. The cardioprotective effects elicited by p66Shc ablation demonstrate the crucial role of mitochondrial ROS formation in ischemia/reperfusion injury. Biochimica et Biophysica Acta (BBA) - Bioenergetics. 2009; 1787:774–780.

Craner MJ, Hains BC, Lo AC, Black JA, Waxman SG. Co-localization of sodium channel Nav1.6 and the sodium-calcium exchanger at sites of axonal injury in the spinal cord in EAE. Brain. 2004a; 127:294–303. [PubMed: 14662515]

Craner MJ, Newcombe J, Black JA, Hartle C, Cuzner ML, Waxman SG. Molecular changes in neurons in multiple sclerosis: altered axonal expression of Nav1.2 and Nav1.6 sodium channels and Na+/Ca2+ exchanger. Proceedings of the National Academy of Sciences. 2004b; 101:8168–8173.

Du H, Guo L, Fang F, Chen D, A Sosunov A, M McKhann G, Yan Y, Wang C, Zhang H, Molkentin JD, Gunn-Moore FJ, Vonsattel JP, Arancio O, Chen JX, Yan SD. Cyclophilin D deficiency attenuates mitochondrial and neuronal perturbation and ameliorates learning and memory in Alzheimer s disease. Nature Medicine. 2008; 14:1097–1105.

Dutta R, McDonough J, Yin X, Peterson J, Chang A, Torres T, Gudz T, Macklin WB, Lewis DA, Fox RJ, Rudick R, Mirnics K, Trapp BD. Mitochondrial dysfunction as a cause of axonal degeneration in multiple sclerosis patients. Annals of Neurology. 2006; 59:478–489. [PubMed: 16392116]

Forte M, Gold BG, Marracci G, Chaudhary P, Basso E, Johnsen D, Yu X, Fowlkes J, Bernardi P, Bourdette D. Cyclophilin D inactivation protects axons in experimental autoimmune encephalomyelitis, an animal model of multiple sclerosis. Proceedings of the National Academy of Sciences. 2007; 104:7558–7563.

Gertz M, Steegborn C. The Lifespan-Regulator p66Shc in Mitochondria: Redox Enzyme or Redox Sensor? Antioxidants & Redox Signaling. 2010a; 13:1417–1428. [PubMed: 20214499]

Gertz M, Steegborn C. The mitochondrial apoptosis pathway and p66Shc: A regulatory redox enzyme or an adapter protein snuggling around? Cell Cycle. 2010b; 9:4425–4426. [PubMed: 21088479]

Giorgio M, Migliaccio E, Orsini F, Paolucci D, Moroni M, Contursi C, Pelliccia G, Luzi L, Minucci S, Marcaccio M, Pinton P, Rizzuto R, Bernardi P, Paolucci F, Pelicci PG. Electron Transfer between Cytochrome c and p66Shc Generates Reactive Oxygen Species that Trigger Mitochondrial Apoptosis. Cell. 2005; 122:221–233. [PubMed: 16051147]

Lin MT, Beal MF. Mitochondrial dysfunction and oxidative stress in neurodegenerative diseases. Nature. 2006; 443:787–795. [PubMed: 17051205]

Lublin F. History of modern multiple sclerosis therapy. Journal of Neurology. 2005; 252:iii3–iii9. [PubMed: 16170498]

Mahad D, Ziabreva I, Lassmann H, Turnbull D. Mitochondrial defects in acute multiple sclerosis lesions. Brain. 2008; 131:1722–1735. [PubMed: 18515320]

Martin LJ, Gertz B, Pan Y, Price AC, Molkentin JD, Chang Q. The mitochondrial permeability transition pore in motor neurons: Involvement in the pathobiology of ALS mice. Experimental Neurology. 2009; 218:333–346. [PubMed: 19272377]

Marracci GH, Jones RE, McKeon GP, Bourdette DN. Alpha lipoic acid inhibits T cell migration into the spinal cord and suppresses and treats experimental autoimmune encephalomyelitis. J Neuroimmunol. 2002; 131:104–114. [PubMed: 12458042]

Migliaccio E, Giorgio M, Mele S, Pelicci G, Reboldi P, Pandolfi PP, Lanfrancone L, Pelicci PG. The p66shc adaptor protein controls oxidative stress response and life span in mammals. Nature. 1999; 402:309–313. [PubMed: 10580504]

Moreira PI, Zhu X, Wang X, Lee HG, Nunomura A, Petersen RB, Perry G, Smith MA. Mitochondria: A therapeutic target in neurodegeneration. Biochimica et Biophysica Acta (BBA) - Molecular Basis of Disease. 2010; 1802:212–220.

Nemoto S, Combs CA, French S, Ahn B-H, Fergusson MM, Balaban RS, Finkel T. The Mammalian Longevity-associated Gene Product p66shc Regulates Mitochondrial Metabolism. Journal of Biological Chemistry. 2006; 281:10555–10560. [PubMed: 16481327]

Noseworthy JH, Lucchinetti C, Rodriguez M, Weinshenker BG. Multiple Sclerosis. New England Journal of Medicine. 2000; 343:938–952. [PubMed: 11006371]

Orsini F, Migliaccio E, Moroni M, Contursi C, Raker VA, Piccini D, Martin-Padura I, Pelliccia G, Trinei M, Bono M, Puri C, Tacchetti C, Ferrini M, Mannucci R, Nicoletti I, Lanfrancone L, Giorgio M, Pelicci P. The life span determinant p66Shc localizes to mitochondria where it associates with mtHsp70 and regulates trans-membrane potential. Journal of Biological Chemistry. 2004; 279:25689–25695. [PubMed: 15078873]

Pinton P, Rimessi A, Marchi S, Orsini F, Migliaccio E, Giorgio M, Contursi C, Minucci S, Mantovani F, Wieckowski MR, Del Sal G, Pelicci PG, Rizzuto R. Protein Kinase C ß and Prolyl Isomerase 1 Regulate Mitochondrial Effects of the Life-Span Determinant p66Shc. Science. 2007; 315:659–663. [PubMed: 17272725]

Rasola A, Bernardi P. The mitochondrial permeability transition pore and its involvement in cell death and in disease pathogenesis. Apoptosis. 2007; 12:815–833. [PubMed: 17294078]

Schinzel AC, Takeuchi O, Huang Z, Fisher JK, Zhou Z, Rubens J, Hetz C, Danial NN, Moskowitz MA, Korsmeyer SJ. Cyclophilin D is a component of mitochondrial permeability transition and mediates neuronal cell death after focal cerebral ischemia. Proceedings of the National Academy of Sciences of the United States of America. 2005; 102:12005–12010. [PubMed: 16103352]

Smith WW, Norton DD, Gorospe M, Jiang H, Nemoto S, Holbrook NJ, Finkel T, Kusiak JW. Phosphorylation of p66Shc and forkhead proteins mediates Aβ toxicity. The Journal of Cell Biology. 2005; 169:331–339. [PubMed: 15837797]

Steinman L. Multiple sclerosis: a two-stage disease. Nat Immunol. 2001; 2:762–764. [PubMed: 11526378]

Su B, Wang X, Zheng L, Perry G, Smith MA, Zhu X. Abnormal mitochondrial dynamics and neurodegenerative diseases. Biochimica et Biophysica Acta (BBA) - Molecular Basis of Disease. 2010; 1802:135–142.

Su K, Banker G, Bourdette D, Forte M. Axonal degeneration in multiple sclerosis: The mitochondrial hypothesis. Current Neurology and Neuroscience Reports. 2009; 9:411–417. [PubMed: 19664372]

Wang W, et al. Superoxide Flashes in Single Mitochondria. Cell. 2008; 134:279–290. [PubMed: 18662543]

Wujek JR, Bjartmar C, Richer E, Ransohoff RM, Yu M, Tuohy VK, Trapp BD. Axon loss in the spinal cord determines permanent neurological disability in an animal model of multiple sclerosis. J. Neuropathol. Exp Neurol. 2002; 61:23–32. [PubMed: 11829341]

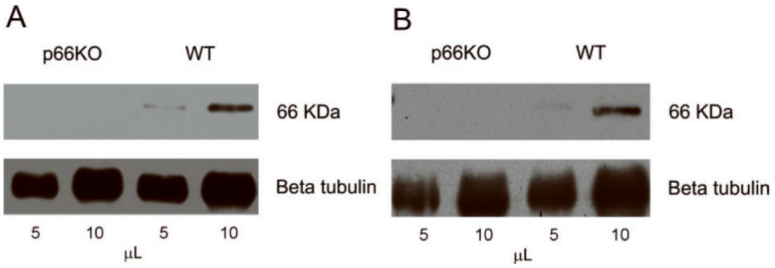

Figure 1. Analysis of p66 expression and elimination in WT and p66-KO nervous tissue and neurons

Lysates prepared from p66-KO and WT mice were immunoprecipitated with anti-Shc antibody on precleared protein G beads. Immunoprecipitates were examined by immunoblot analysis probing with the anti-Shc BG8 antibody. Immunoblots were re-probed with beta tubulin as a protein loading control. Blot analysis showed p66 expression in WT brain cortical lysates and elimination in those prepared from p66-KO mice (A). Similar results were shown in hippocampal neuronal lysates (B).

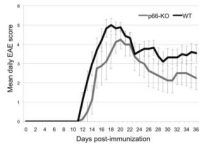

Figure 2. p66-KO mice showed less severe clinical EAE compared to WT mice

Immunized p66-KO and WT mice were scored daily for clinical signs of weakness and paralysis over a 36-day observation period. Throughout the entire clinical course, mean p66-KO scores were less than the WT scores. At the end of the 36 days, the p66-KO mice had significantly lower scores compared to the WT mice, reflecting the overall trend of reduced clinical impairment.

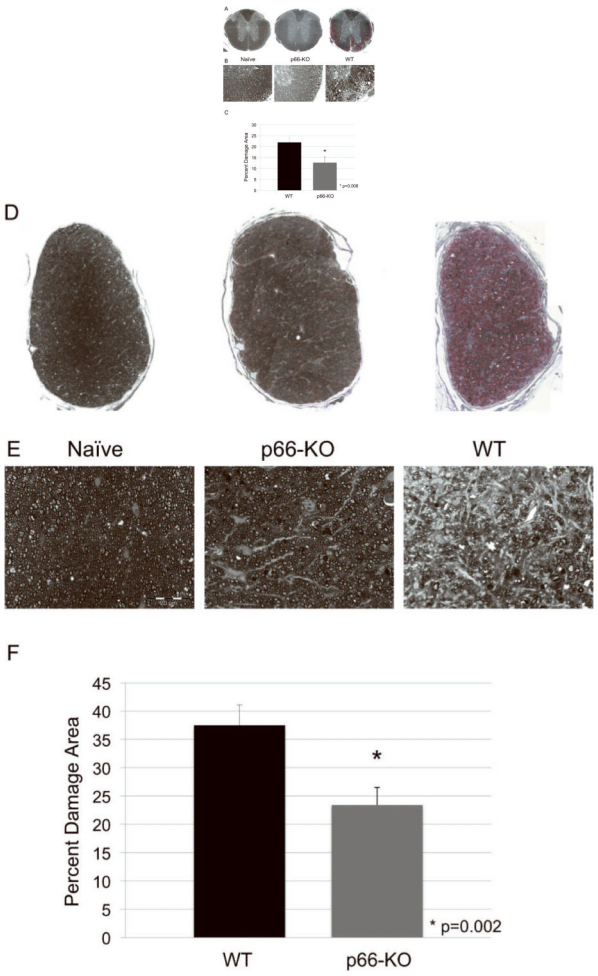

Figure 3. p66-KO mice showed less axonal damage than WT mice following EAE induction

A) Lower power view of plastic-embedded toluidine-blue stained thoracic spinal cord sections from representative naïve (left), p66-KO (middle), and WT (right) mice 36 days following EAE induction. Red indicates circled areas of damage. B) Higher power view of sections. Note the greater preservation of axonal integrity in the p66-KO mice compared to WT mice. C) p66-KO mice showed a significant 42% reduction in ventrolateral white matter damage compared to WT mice. D) Lower power view of plastic-embedded toluidine-blue stained optic nerve sections from representative naïve (left), p66-KO (middle), and WT (right) mice 36 days following EAE induction. Red indicates circled areas of damage. E) Higher power view of sections. Note the greater preservation of axonal integrity in the p66-KO mice compared to WT mice. F) p66-KO mice showed a significant 38% reduction in optic nerve damage compared to WT mice.

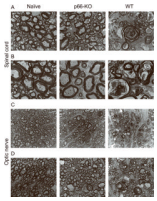

Figure 4. Electron microscopy of p66-KO and WT nervous tissue illustrates axonal protection associated with p66 elimination

Electron microscopy images of naïve (left), p66-KO (middle), and WT (right) ultrathin sections from plastic embedded thoracic spinal cords (A,B) and optic nerves (C,D) imaged at 4800× (A,C) and 9300× (B,D). Greater axonal preservation was observed in the p66-KO images in comparison to the WT images.

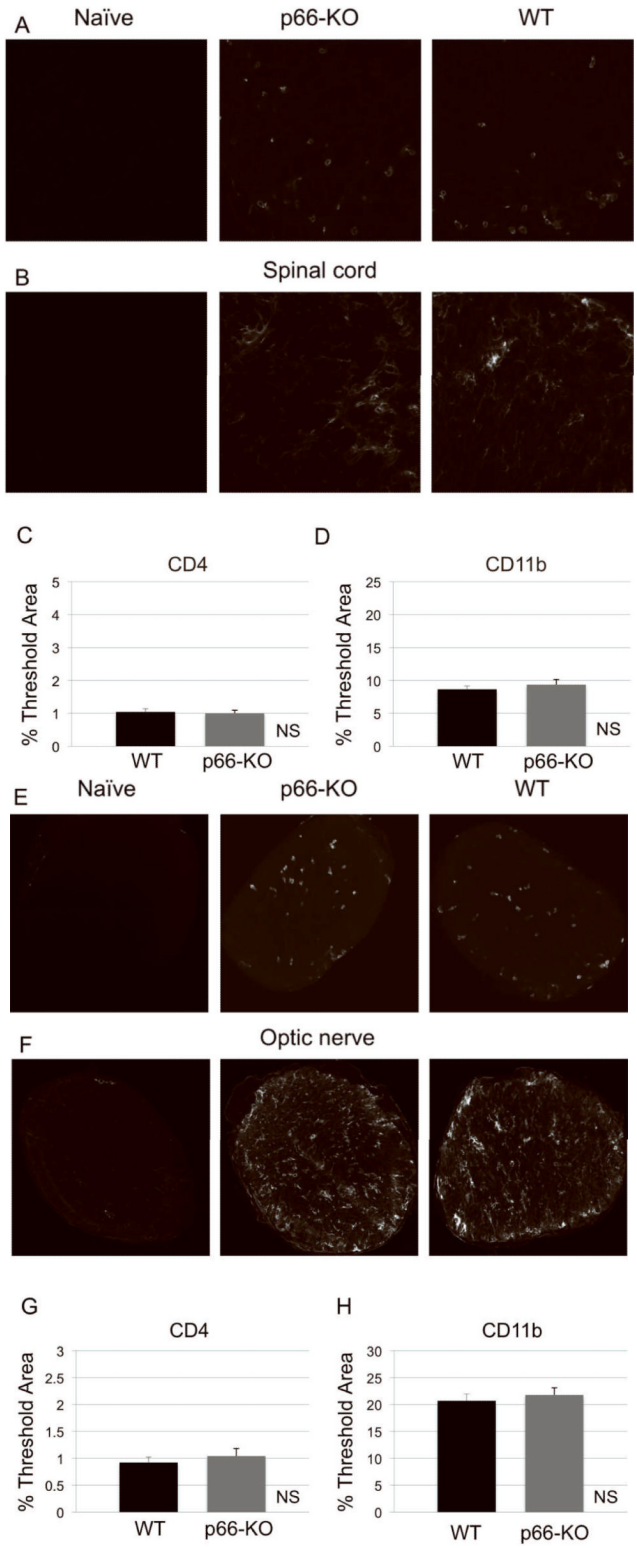

Figure 5. p66-KO nervous tissue showed similar levels of immune cell infiltration compared to WT tissue following EAE induction

Naïve (left), p66-KO (middle), and WT (right) lumbar spinal cord sections 36 days following EAE induction were stained for T cells with CD4 antibody (A) and for

macrophages/microglia with CD11b antibody (B). Quantification of immune cell infiltration showed no significant difference between the p66-KO and WT groups (C,D). Naïve (left), p66-KO (middle), and WT (right) optic nerve sections 36 days following EAE induction were stained for T cells with CD4 antibody (E) and for macrophages/microglia with CD11b antibody (F). Quantification of immune cell infiltration showed no significant difference between the p66-KO and WT groups (G,H). NS = difference not significant ($p>0.05$).

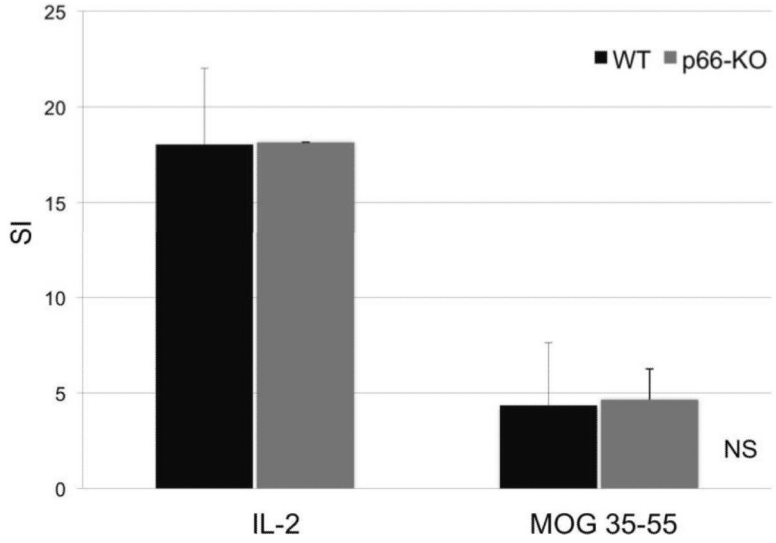

Figure 6. T cell proliferation studies showed no significant differences between p66-KO and WT mice in MOG immunoreactivity

Using standard EAE protocol, p66-KO and WT mice were immunized with MOG 35-55 peptide. Ten days post-immunization, lymph nodes were collected for proliferation studies. Lymph node cultures treated with positive control IL-2 and MOG 35-55 peptide (25mg/mL) showed no significant differences in proliferative responses between the p66-KO and WT groups. SI = Stimulation index; NS = difference not significant ($p>0.05$).

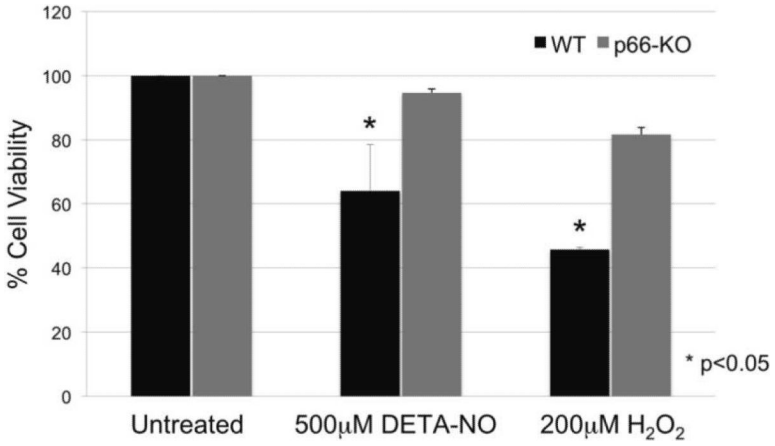

Figure 7. p66-KO neurons showed greater protection following treatment with oxidative insults implicated in EAE and MS neurodegenerative pathways

p66-KO neurons had a significantly greater cell viability percentage compared to WT neurons when treated for 15 minutes with either A) 500μ-M of DETA-NO or B) 200 μ-M H_2O_2. Cell counts were obtained 24 hours post treatment. A) DETA-NO treated p66-KO neurons had a mean cell viability of 94.7±1.2% compared to 64.0±14.6% for the WT neurons (p=0.04). B) H_2O_2 treated p66-KO neurons had a mean cell viability of 81.7±2.2% compared to 45.7±0.7% for the WT neurons (p=0.02). (n per treatment/genotype = 3 cultures; 4 plates/culture)

Table 1

Cytokine studies showed no significant differences between p66-KO and WT mice with EAE

Using standard EAE protocol, p66-KO and WT mice were immunized with MOG 35-55 peptide. Ten days post-immunization, lymph nodes were collected for cytokine studies. Lymph node cultures treated with control media and MOG 35-55 (25mg/mL) peptide for 48 hours, and cell culture supernatants were collected for analysis using the Luminex Bio-Plex mouse cytokine assay kit. Results showed no significant differences between the p66-KO and WT groups for Th1 (a), Th2 (b), or Th17 (c) cytokine levels.

a) Th1 cytokines

	Media (pg/mL)	f/p values	25 mg MOG (pg/mL)	f/p values
TNF-alpha	p66-KO: 265.96±101.17 WT: 272.28±64.37	*z=0.244949* *p=0.403*	p66-KO: 465.04±139.72 WT: 414.03±85.63	*z=0.734847* *p=0.231*
IFN-gamma	p66-KO: 375.99±316.72 WT: 429.54±193.00	*z=0.734847* *p=0.231*	p66-KO: 11033.38±2625.10 WT: 15348.21±2563.96	*z=0.734847* *p=0.231*

b) Th2 cytokines

	Media (pg/mL)	f/p values	25 mg MOG (pg/mL)	f/p values
IL-4	p66-KO: 7.56±7.15 WT: 9.50±5.72	*z=0.774597* *p=0.219*	p66-KO: 21.60±24.39 WT: 19.63±16.20	*z=0.489898* *p=0.312*
IL-10	p66-KO: 50.40±47.59 WT: 43.27±41.53	*z=0.57735* *p=0.282*	p66-KO: 110.73±96.04 WT: 89.23±69.92	*Z=0.57735* *p=0.282*

c) Th17 cytokines

	Media (pg/mL)	f/p values	25 mg MOG (pg/mL)	f/p values
IL-17	p66-KO: 3237.60±2232.62 WT: 4574.22±1121.16	*z=0* *p=0.5*	p66-KO: 13198.57±4259.96 WT: 14555.54±4526.26	*z=1.44338* *p=0.074*